Journal of Solid State Chemistry 181 (2008) 2185–2190

Contents lists available at ScienceDirect

Journal of Solid State Chemistry

journal homepage: www.elsevier.com/locate/jssc

Synthesis and structural investigation of a new oxide fluoride of composition $Ba_2SnO_{2.5}F_3 \cdot xH_2O$ ($x \approx 0.5$)

Frank J. Berry [a], Elaine Moore [a], Michael Mortimer [a,*], Xiaolin Ren [a], Richard Heap [b], Peter Slater [b], Michael F. Thomas [c]

[a] Department of Chemistry and Analytical Sciences, The Open University, Walton Hall, Milton Keynes MK7 6AA, UK
[b] Department of Chemistry, University of Surrey, Guildford, Surrey GU2 7XH, UK
[c] Department of Physics, University of Liverpool, Liverpool L69 3BX, UK

ARTICLE INFO

Article history:
Received 12 March 2008
Received in revised form
8 May 2008
Accepted 12 May 2008
Available online 18 May 2008

Keywords:
Oxide fluoride
Perovskite-related structure
Fluorine MAS NMR spectroscopy
Atomistic computer modelling
EXAFS
XANES

ABSTRACT

The preparation of a new oxide fluoride of composition $Ba_2SnO_{2.5}F_3 \cdot xH_2O$ ($x \approx 0.5$) from the low-temperature (240 °C) reaction between Ba_2SnO_4 and ZnF_2 is reported. X-ray and neutron powder diffraction showed fluorination to result in a significant enlargement along the *c*-axis (by ca. 3 Å) of the unit cell of the precursor oxide. A structural model based on the perovskite-related K_2NiF_4-type structure of this oxide is proposed in which there is direct replacement of oxygen in octahedral SnO_6 units by fluorine, as well as the presence of F^- at interstitial sites between BaO rock salt layers. Atomistic computer modelling indicates that apical fluorine substitution is favoured. The structural model is supported by the results of ^{19}F and ^{119}Sn MAS NMR spectroscopy as well as tin K- and barium K-edge EXAFS. Thermal analysis revealed the presence of water in the synthesized material and this is assigned to interstitial sites. ^{119}Tin Mössbauer spectroscopy and tin K-edge XANES are consistent with enhanced withdrawal by substituted fluorine of electron density from Sn^{4+}.

1. Introduction

The preparation and characterization of inorganic oxide fluorides with perovskite-related structures has attracted attention in recent years largely as a result of interest in changing the structural and physical properties of high T_c copper oxide superconductors [1–3]. Oxides with a K_2NiF_4-type structure, particularly those containing transition metals with variable oxidation states such as in materials relating to cuprates, ferrates and manganates [4–9], have also been the subject of fluorination and the approach has more recently been successfully extended to the compound Ba_2ZrO_4 where there is no possibility for a change in oxidation state [10]. We report here on the fluorination of the perovskite-related K_2NiF_4-type compound Ba_2SnO_4 through a low-temperature (240 °C) reaction with ZnF_2 and describe the structural properties of the resultant fluorinated material of composition $Ba_2SnO_{2.5}F_3 \cdot xH_2O$ ($x \approx 0.5$).

2. Experimental

The compound Ba_2SnO_4 was prepared by calcination of a well ground mixture of appropriate quantities of high-purity barium (II) carbonate and tin (IV) oxide at 1250 °C for 24 h in air. Fluorination was achieved by mixing Ba_2SnO_4 with anhydrous zinc difluoride in a 1:1.5 molar ratio and heating the mixture at 240 °C for 24 h in flowing nitrogen. ICP-AES analysis performed by Medac Ltd. of the final mixture (containing the fluorinated phase and ZnO from the fluorinating agent) gave barium and tin contents of 43.9 and 20.3 wt%, respectively. This confirms, to an acceptable level of agreement, that there is no change in Ba:Sn ratio during the fluorination process. Thermal analysis of the same material was performed using a Rheometric Scientific STA 1500 instrument using flowing dry nitrogen (60 ml min^{-1}) and a heating rate of 10 °C min^{-1}. X-ray powder diffraction patterns were recorded with a Siemens D5000 diffractometer in reflection mode using Cu-$K\alpha$ radiation at ambient temperature. Time-of-flight neutron diffraction data were collected on the diffractometer POLARIS at the ISIS, Rutherford Appleton Laboratory. Structure refinement was performed using the GSAS suite of Rietveld refinement software [11].

The NMR spectrometers used were a Varian Unity Inova NMR spectrometer operating at 282.09 MHz for ^{19}F and a Varian InfinityPlus operating at 186.23 MHz for ^{119}Sn. All measurements were made at ambient temperature. Direct polarization ^{19}F MAS NMR spectra were recorded with sample spinning rates in the range 10–20 kHz and recycle delays of 10 s. ^{119}Sn MAS NMR spectra were recorded with ^{19}F decoupling, a sample spinning rate of 14 kHz and recycle delays of 120 s. Chemical shifts are quoted

* Corresponding author. Fax: +44 1908 858 327.
E-mail address: m.mortimer@open.ac.uk (M. Mortimer).

0022-4596/$ - see front matter © 2008 Elsevier Inc. All rights reserved.
doi:10.1016/j.jssc.2008.05.015

relative to $CFCl_3$ and $Sn(CH_3)_4$ for ^{19}F and ^{119}Sn, respectively. It can be noted that only a small residual resonance corresponding to ZnF_2, $\delta(^{19}F) = -203.9$ (less than 4% total integrated intensity), was observed in the ^{19}F MAS NMR spectra confirming that most of the ZnF_2 is utilized in the fluorination process.

Barium and tin K-edge X-ray absorption spectra were recorded at the Synchrotron Radiation Source at Daresbury Laboratory UK with an average current of 200 mA at 2 GeV. The data were collected in transmission geometry on Station 9.2 from samples in the form of pressed discs at 298 and 77 K. The edge profiles were separated from the EXAFS data and, after subtraction of a linear pre-edge background, normalized to the edge step. The position of the X-ray absorption edge was defined as the energy at which the normalized absorption was 0.5, that is the absorption at half-height of the edge step. The EXAFS oscillations were isolated after background subtraction of the raw data using the Daresbury programme EXBACK and converted into k space. The data were weighted by k^3, where k is the photoelectron wave vector, to compensate for the diminishing amplitude of EXAFS at high k. The data were fitted using the Daresbury programme EXCURV98 [12].

^{119}Tin Mössbauer spectra were recorded at 77 K with a constant acceleration spectrometer using a ca. 25 mCi $Ca^{119}SnO_3$ source. The ^{119}Sn Mössbauer chemical isomer shift data are quoted relative to SnO_2.

Atomistic computer modelling calculations were performed using the programme GULP [13] with Buckingham potentials used for all atoms. The potentials for Ba–O, Sn–O and O–O were taken from those used in a study of $BaSnO_3$ [14] and those for Ba–F, Sn–F, O–F and F–F, which are relevant to fluorinated models of Ba_2SnO_4, were derived using the structures of BaF_2, SnF_4, SrF_2, Sr_3GaO_4F and properties of BaF_2. The values of all parameters are given in Table 1. Calculated lattice parameters are compared with experimental values in Table 2.

3. Results and discussion

The 1:1.5 molar reaction between Ba_2SnO_4 and ZnF_2 is consistent with the formation of $Ba_2SnO_{2.5}F_3$, with the presence of ZnO resulting from the decomposition of the fluorinating agent. In addition, thermal analysis showed that the final fluorinated product underwent a mass loss of ca. 1.6% over the temperature range 25–600 °C. This mass loss, which is comparable to that recorded from fluorinated Ba_2ZrO_4 which was also prepared using ZnF_2 as the fluorinating agent [10], can be associated with the loss of $\sim 0.5 \cdot H_2O$ incorporated within the structure of the fluorinated compound via absorption of water from the atmosphere. The ready ability of Ba-containing K_2NiF_4 phases to incorporate water has been reported previously [15]. We thus propose that the composition of the new oxide fluoride is $Ba_2SnO_{2.5}F_3 \cdot 0.5H_2O$. If, as is likely, the incorporation of H_2O within the structure gives rise to OH^- anions, then a formulation as $Ba_2SnO_2(OH)F_3$ is also possible [10].

The X-ray powder diffraction patterns recorded from Ba_2SnO_4 and its fluorinated derivative are shown in Fig. 1.

The pattern recorded from Ba_2SnO_4, space group $I4/mmm$, is consistent with other studies reported in the literature [16–18] and yields lattice parameters $a = b = 4.140(1)$ Å and $c = 13.309(1)$ Å. The fluorinated phase showed a shift in some Bragg peak positions to lower angle corresponding to a change in lattice parameters such that $a = b = 4.080(1)$ Å and $c = 16.330(1)$ Å. The result demonstrates a significant enlargement of the Ba_2SnO_4 unit cell along the c-axis following fluorination and is consistent, as found [10] in the investigation of fluorinated isostructural Ba_2ZrO_4, with the occupation by

Table 2
Calculated and experimental cell parameters

	a (Å)	c (Å)
BaF_2		
Experimental	6.2001	
Calculated	6.2001	
SnF_4		
Experimental	4.0498	7.9375
Calculated	4.0769	8.0212
Ba_2SnO_4		
Experimental	4.1411	13.2834
Calculated	4.1180	13.1413

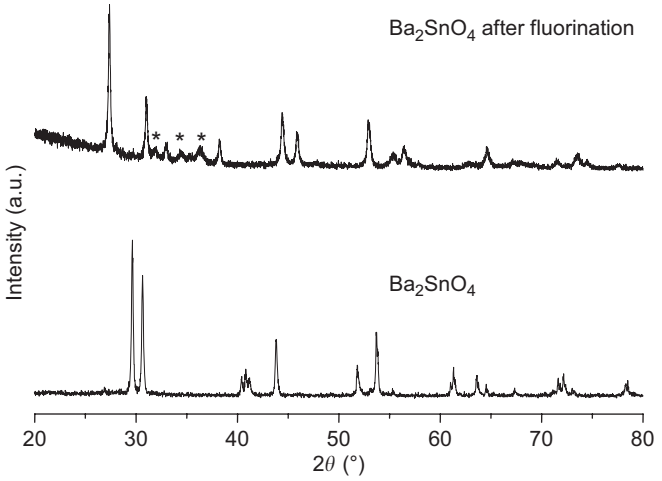

Fig. 1. X-ray powder diffraction patterns recorded from Ba_2SnO_4 and its fluorinated derivative. ZnO is present due to the decomposition of the fluorinating agent and the main peaks are marked (*).

Table 1
Interatomic potentials

Potential	A (eV)	ρ (Å)	C (eV Å^6)	Spring constant (k) (eV Å^{-2})	Shell charge (e)
O shell–O shell	9547.960	0.2192	32.00		
Ba shell–O shell	873.82901	0.3863	0.0		
Sn shell–O shell	1056.8	0.3683	0.0		
F shell–F shell	10114.28297	0.365174	2422.12686		
Ba shell–F shell	9111.02809	0.2795	0.0		
Sn shell–F shell	27630696.20204	0.115456	0.0		
O shell–F shell	464.54	0.3362	22.10		
Ba core–Ba shell				459.2	9.203
Sn core–Sn shell				2037.8	1.58
O core–O shell				23.09	−2.389
F core–F shell				101.2	−2.38

fluorine of interstitial sites between the BaO rock salt layers in the K_2NiF_4-type structure of Ba_2SnO_4. It is also reasonable to assume [10] that the fluorination process involves substitution; that is direct replacement of oxygen in the octahedral SnO_6 units by fluorine.

A more-detailed analysis was carried out using the neutron powder diffraction data (Fig. 2), although the structure refinement is complicated by the presence of additional phases: ZnO from the fluorinating agent and a small amount of BaF_2. Both of these phases were included in the refinement. As a result of the particularly large ZnO diffraction peaks, the refinement results are only employed here to add support for conclusions concerning the occupancy of interstitial sites. It can be noted that the MAS NMR, EXAFS and Mössbauer results are not affected by the presence of ZnO. The structural refinement gave a good fit to the data (Fig. 2) and suggested that there were displacements of the K_2NiF_4-type equatorial (label 1) and axial (label 2) anions off their ideal sites, consistent with small displacements caused by the introduction of interstitial F^-. The final refinement suggested nearly full occupancy of both the normal anion sites and the interstitial sites: the ideal K_2NiF_4 structure sites (O1/F1, O2/F2) refined to full occupancy (and so were fixed at this value in the final refinement), while there was a small number of vacancies in the interstitial sites (O3/F3). The total anion occupancy refined to a value of 5.86(4), which is close to the value of 6 for the composition $Ba_2SnO_{2.5}F_3 \cdot 0.5H_2O$ proposed for the fluorinated derivative. It was not possible to locate H sites within the structure and this can possibly be correlated with a range of sites involving thermal motion, coupled with the low magnitude of the scattering factor for H. More-detailed low-temperature neutron diffraction investigations, with H/D exchange, would be required in this respect. The final refined parameters are given in Table 3, with selected bond distances in Table 4. Due to the similar scattering factors for O and F it is not possible to distinguish between the two by neutron diffraction (or indeed by X-ray diffraction).

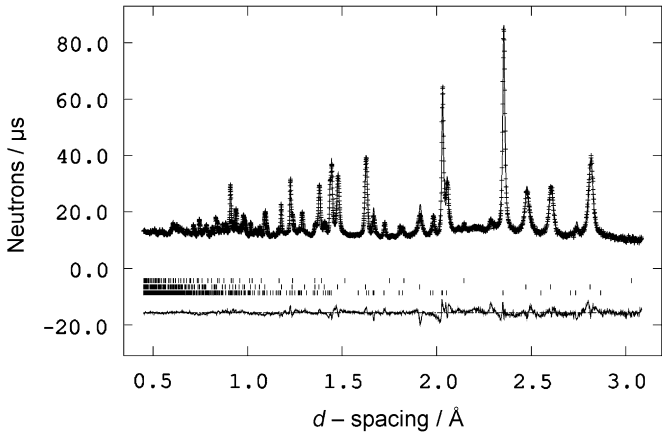

Fig. 2. Observed, calculated and difference neutron diffraction profiles of $Ba_2SnO_{2.5}F_3 \cdot xH_2O$ ($x \approx 0.5$). (Lower tick marks = $Ba_2SnO_{2.5}F_3 \cdot xH_2O$ ($x \approx 0.5$); middle tick marks = ZnO (from the fluorinating agent); upper tick marks = BaF_2.)

The inclusion of both interstitial and substitutional fluorine in the fluorinated derivative of Ba_2SnO_4 is supported by ^{19}F MAS NMR spectroscopy. The ^{19}F MAS NMR spectrum recorded at a spinning rate of 14.0 kHz for this derivative is shown in Fig. 3. (Spectra recorded at different sample spinning rates were used to confirm the presence of spinning sidebands.) There are two distinct sets of resonances: an asymmetric resonance centred at −82.4 p.p.m. and a group of overlapping resonances (−18.1, −7.7 and 2.9 p.p.m.) at higher frequency. Significantly, the relative intensities (including spinning sidebands) of these two sets are in a ratio that is close to 1:1. The resonance at −82.4 p.p.m. is assigned to substitutional fluorine since it lies in a region (−40 to −100 p.p.m.) that is typical of ^{19}F resonances in SnF_2-type environments [19,20]. The asymmetric nature of this resonance may be due to the possibility of single- or double-fluorine substitution within a single SnO_6 unit. The higher frequency group of resonances is assigned to interstitial F^- in sites of varying local order but generally within environments in the close vicinity of Ba atoms in the BaO rock salt layers of the structure; in this case, direct comparison can be made with the ^{19}F resonance of BaF_2 (ca. −15 p.p.m. [21]). This comparative approach to assignment is similar to that used by Du et al. [22] in a ^{19}F MAS NMR investigation of $Ba_2WO_3F_4$. (The presence of a small amount of BaF_2, as found in the neutron powder diffraction pattern, cannot be discounted since the single ^{19}F resonance for BaF_2 would be difficult to resolve from the higher intensity, overlapping interstitial resonances.) It can be noted that the resonance at 2.9 p.p.m. is particularly affected by sample spinning rate undergoing a linewidth reduction from $\Delta\upsilon_{1/2} \approx 3.5$ to 2.2 kHz with an increase in spinning rate from 12.5 to 14.0 kHz. We suggest that this is due to the removal of homonuclear coupling contributions. This selective behaviour provides further evidence that the three resonances assigned to interstitial F^- correspond to different patterns of occupation of the available sites. In addition, the possibility of occupation of interstitial sites by OH anions cannot be excluded. Overall, the ^{19}F MAS NMR results indicate that the number ratio of substitutional to interstitial fluorine in the unit cell ($Z = 2$) of the fluorinated derivative is 3:3.

The ^{119}Sn MAS NMR spectrum of the fluorinated derivative (not shown) consists of a single, relatively broad ($\Delta\upsilon_{1/2} \approx 3.2$ kHz),

Table 4
Selected bond distances

Bond	Bond distance (Å)
Sn–O1/F1	2.0379(3)
Sn–O2/F2	2.044(3)
Ba–O1/F1	3.331(4), 3.052(4)
Ba–O2/F2	3.093(5), 2.9084(7), 2.711(5)
Ba–O3/F3	2.615(2)

Table 3
Refined structural parameters from neutron diffraction[a]

Atom	Site	x	y	z	$100 \times U_{iso}$ (Å^2)	Site occupancy
Ba	4*e*	0	0	0.3503(2)	0.83 (6)	1.0
Sn	2*a*	0	0	0	0.53 (5)	1.0
O1/F1	8*g*	0	0.5	0.0110(2)	0.56 (6)	0.5
O2/F2	16*m*	0.0337(8)	0.0337(8)	0.1238(2)	0.43 (8)	0.25
O3/F3	4*d*	0	0.5	0.25	1.2 (1)	0.93(2)

[a] *I*4/*mmm*; $a = b = 4.0596(1)$ Å, $c = 16.4329(9)$ Å; $R_{wp} = 2.75\%$, $R_p = 3.99\%$.

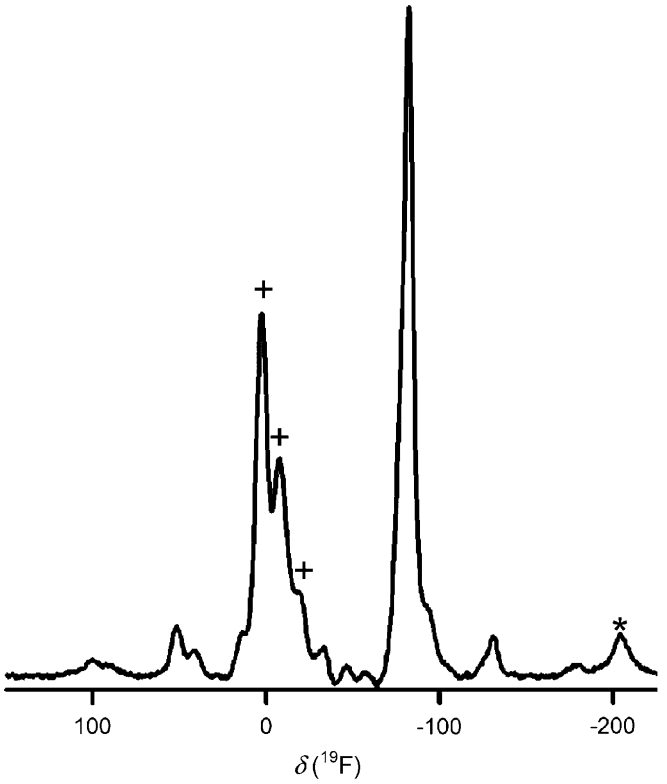

Fig. 3. ^{19}F MAS NMR spectrum of the fluorinated derivative (sample spinning rate = 14.0 kHz). The group of overlapping resonances at −18.1, −7.7 and 2.9 p.p.m. are marked (+). The resonance at −203.9 p.p.m. (*) corresponds to residual ZnF_2. Spinning sidebands were identified by experiments at different sample spinning rates.

resonance at −715 p.p.m. (A low intensity resonance at −593 p.p.m. corresponding to a residual amount of non-substituted SnO_6 units is also present.) The resonance at −715 p.p.m. can be compared with that of −803 p.p.m. recorded for $[SnF_6]^{2-}$ in dichloromethane solution at −100 °C [23] (assuming that the solid-state value for $[SnF_6]^{2-}$ will be similar). This comparison suggests that increasing substitution of oxygen by fluorine in SnO_6 units does not result in major ^{119}Sn chemical shift differences. In this context, it can be noted that ^{119}Sn NMR studies [24] in aqueous solution of $[SnCl(H_2O)_5]^{3+}$ have reported $\delta(^{119}Sn) = -620$ p.p.m., which can be compared with values of $\delta(^{119}Sn) = -623$ to −627 p.p.m. for the di-substituted *cis* and *trans* cations, $[SnCl_2(H_2O)_4]^{2+}$. Although the evidence is not definitive, it is not unreasonable to suggest that the broad ^{119}Sn resonance observed for the fluorinated derivative ($\Delta\upsilon_{1/2} \approx 17$ p.p.m. at the frequency of recording) could represent contributions from both single- and double-fluorine substituted SnO_6 units and, in this respect, is consistent with the interpretation of the corresponding ^{19}F NMR spectrum.

Computer modelling provides further structural information particularly with regards to the substitutional sites. Two models, both of the dehydrated form of $Ba_2SnO_{2.5}F_3$ were considered with the interstitial sites located at (0, 0.5, 0.25) (see Fig. 4). In one model (A), the fluorine occupancies of the interstitial and substitutional sites were set at 0.75 and 0.375, respectively. Different arrangements for the substitution of equatorial (O1) and apical (O2) sites were then considered. The other model (B) is similar but takes into account the possibility of reduced occupancy of O2 sites to give vacancies [10]. In the model, these are created by the transfer of O^{2-} from apical sites to interstitial sites. The results of the computer modelling are given in Table 5

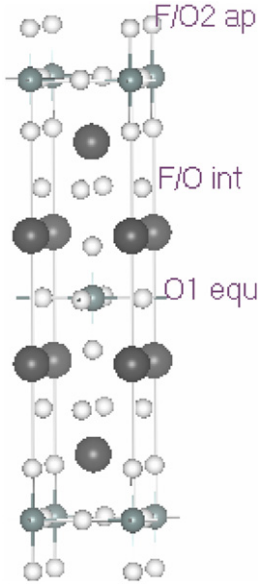

Fig. 4. A structural model for the dehydrated form of $Ba_2SnO_{2.5}F_3$ (large dark spheres = Ba; small dark spheres = Sn). Interstitial sites are labelled 'F/O int', substitutional apical sites in SnO_6 are labelled 'F/O2 ap' and equatorial oxygen sites in SnO_6 are labelled 'O1 equ'.

Table 5
Calculated energies and cell parameters for $Ba_2SnO_{2.5}F_3$

Model[a]	Substitution pattern for fluorine[a]	*a* (Å)	*c* (Å)	Lattice energy (eV)
A	O1 only	4.10	18.10	−167.1077
	O2 only	4.07	17.55	−168.5761
	O1 and O2	4.08	17.76	−166.3382
B	O1 only	4.13	18.75	−164.0700
	O2 only	4.09	17.53	−166.2608
	O1 and O2	4.11	18.17	−161.4372

[a] See text for further details.

where for the second model the occupancy of the interstitial sites is complete with F^- and O^{2-} in the ratio 3:1. It is significant for both models, which represent plausible limits for vacancy-type structures, that the lowest energy is found for apical (O2) substitution only. Furthermore, the cell parameter *c* is at its lowest value for this type of substitution. Overall, we conclude that apical substitution is favoured in the fluorination process. It is worth noting that we found that all models optimized with a *c* value greater than that observed experimentally. This may be due to the fact that water has not been explicitly included in the modelling. It is possible that the protonation of remaining apical oxygens would lead to a reduction in cell length.

Tin and barium K-edge EXAFS recorded at 298 K from Ba_2SnO_4 and its fluorinated derivative are shown in Fig. 5 and the best-fit parameters are collected in Table 6.

The tin and barium K-edge EXAFS data recorded from Ba_2SnO_4 were fitted to a model derived from X-ray powder diffraction data [14] for Ba_2SnO_4. The tin K-edge EXAFS recorded from the fluorinated derivative show internuclear distances similar to those in Ba_2SnO_4. The small reduction in the first shell Sn–O distance on fluorination is consistent with results found when the analogous compound Ba_2ZrO_4 was fluorinated [10]. As to be expected, more significant changes occur in the barium K-edge EXAFS on fluorination. The EXAFS fit a model consisting of two shells of four oxygen, or fluorine, atoms (O/F) at 2.640 and 2.908 Å with a further shell of four oxygen atoms at 3.178 Å. The first shell

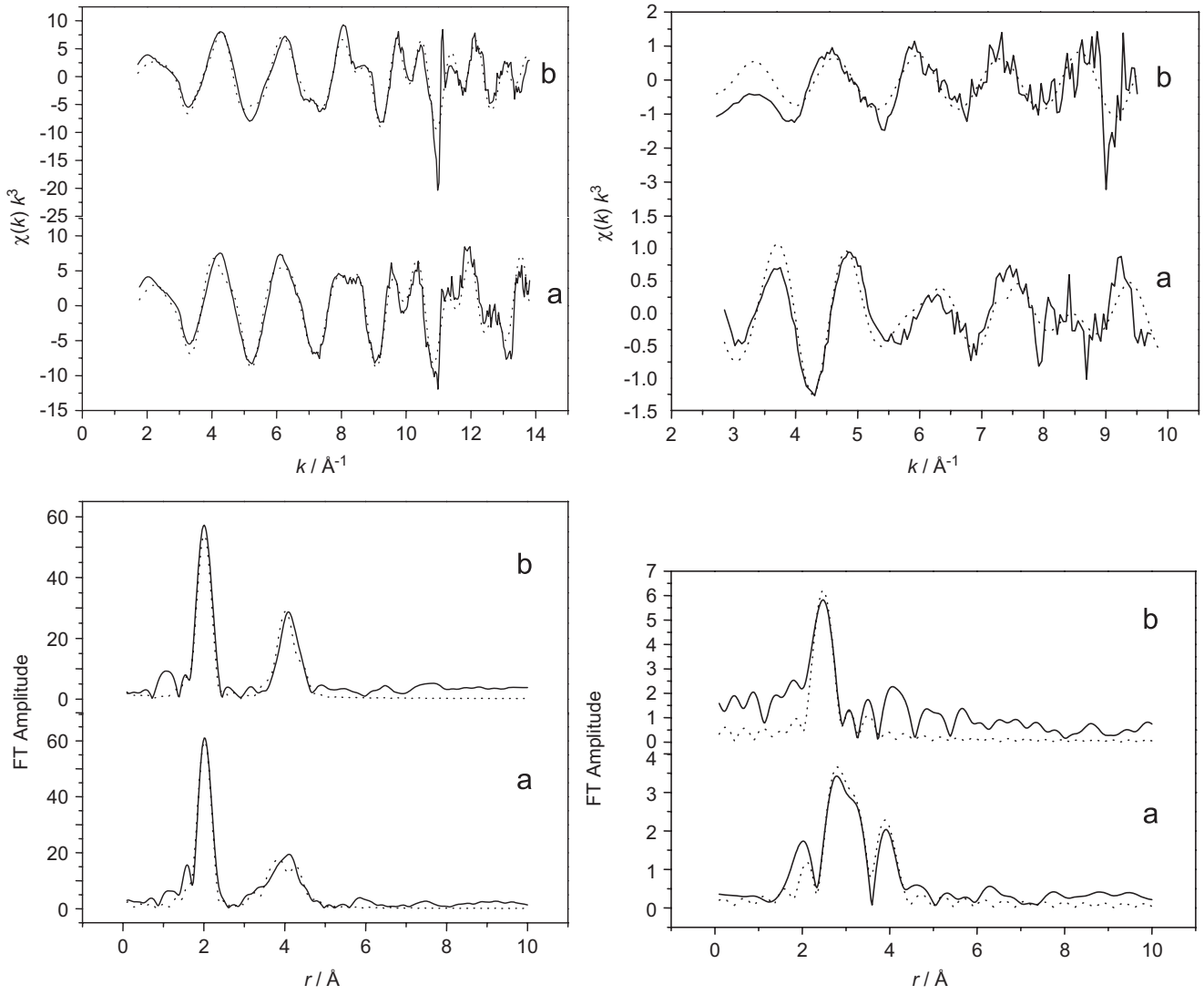

Fig. 5. k^3-Weighted tin (left-hand column) and barium (right-hand column) K-edge EXAFS and the corresponding Fourier transforms recorded at 298K from (a) Ba_2SnO_4 and (b) its fluorinated derivative. The experimental data are indicated by solid lines and dotted lines indicate the best fit to the data.

Table 6
Final fitted parameters obtained from tin K-edge and barium K-edge EXAFS data recorded at 298 K

Tin K-edge				Barium K-edge			
Atom type	Coordination number	Sn-atom distance (±1%) (Å)	$2\sigma^2$ (Å^2) (±10%)	Atom type	Coordination number	Ba-atom distance (±1%) (Å)	$2\sigma^2$ (Å^2) (±10%)
Ba_2SnO_4							
O	6	2.054	0.006	O	1	2.553	0.012
Ba	8	3.556	0.027	O	4	2.806	0.012
Sn	4	4.237	0.010	O	4	3.010	0.015
O	16	4.593	0.016	Sn	4	3.597	0.041
Ba_2SnO_4/F							
O	6	2.029	0.010	O/F	4	2.640	0.014
Ba	8	3.499	0.028	O/F	4	2.908	0.016
Sn	4	4.152	0.002	O	4	3.178	0.035

can be attributed to O/F at interstitial positions (0, 0.5, 0.25). The coordination number is consistent with full occupation of the interstitial sites in agreement with conclusions drawn from the structure refinement based on the neutron diffraction data, but is should also be recognized that the ^{19}F NMR results suggest that there are different patterns of occupation of these sites. The shells at 2.908 and 3.178 Å correspond to O/F at O2 sites and oxygen at O1 sites; the corresponding distances in Ba_2SnO_4 are 3.010 and 2.806 Å, respectively. We interpret these changes as being associated with the increasing anionic content of the unit cell

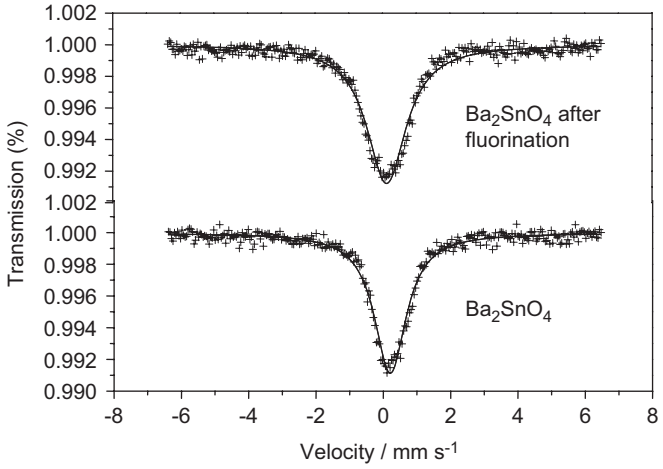

Fig. 6. ^{119}Sn Mössbauer spectra recorded from Ba_2SnO_4 and its fluorinated derivative at 77 K.

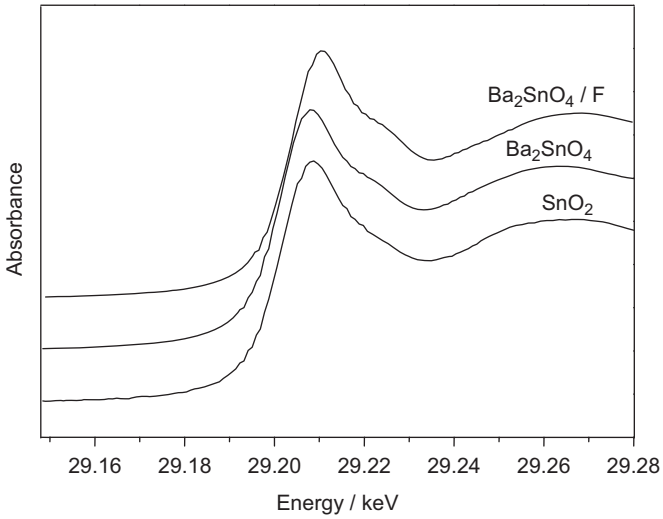

Fig. 7. Tin K-edge XANES recorded from SnO_2, Ba_2SnO_4 and its fluorinated derivative (denoted as Ba_2SnO_4/F) at 77 K.

due to the incorporation of interstitial F^- and a consequent displacement of Ba^{2+} towards these sites. The Ba–O distance for the single oxygen at 2.553 Å in Ba_2SnO_4 increases on fluorination so that its value is greater than that of the fitted shells.

The ^{119}Sn Mössbauer spectrum recorded from Ba_2SnO_4 at 77 K was composed of a single absorption, $\delta = 0.22(1)\,\mathrm{mm\,s^{-1}}$, and the spectrum recorded from the fluorinated derivative was similar but with a smaller chemical isomer shift, $\delta = 0.12(1)\,\mathrm{mm\,s^{-1}}$, indicative of the electron withdrawing effect of fluorine on the electron density around Sn^{4+} (Fig. 6). This result is endorsed by tin K-edge XANES (Fig. 7 and Table 7) also recorded at 77 K. The X-ray absorption edge position of the fluorinated derivative is observed at a higher energy than that for Ba_2SnO_4 for which the XANES is identical to that for tin dioxide. These results are consistent with electronegative fluorine withdrawing electron density from Sn^{4+}.

In summary, we have shown that the K_2NiF_4-type phase Ba_2SnO_4 can be fluorinated at 240 °C using ZnF_2. The new oxide fluoride $Ba_2SnO_{2.5}F_3 \cdot 0.5H_2O$ is prepared when these reactants are in the molar ratio 1:1.5. All of the available evidence is consistent with a structural model in which fluorine occupies both interstitial sites between the BaO rock salt layers, as well as substitutional sites in SnO_6 units, of the precursor oxide. Computer modelling indicates that apical substitution is favoured. Overall, the results provide a further example of the applicability of low-temperature routes for the synthesis of new oxide fluoride compounds.

Table 7
Tin K-edge XANES recorded at 77 K

Compound	Edge position (±0.2) (eV)
Sn metal	29200.0
SnO_2	29202.3
Ba_2SnO_4	29202.3
Ba_2SnO_4/F	29205.7

Acknowledgments

We thank Dr. D. Apperley and the EPSRC National Solid-state NMR Research Service at the University of Durham for ^{19}F and ^{119}Sn MAS NMR spectra and useful advice. We also thank ISIS, Rutherford Appleton Laboratory, for the provision of neutron diffraction beamtime and R. Smith for help with the collection of the neutron diffraction data.

References

[1] M.G. Francesconi, C. Greaves, Supercond. Sci. Techol. 10 (1997) A29.
[2] C. Greaves, M.G. Francesconi, Curr. Opin. Solid State Mater. Sci. 3 (1998) 132.
[3] E.E. McCabe, C. Greaves, J. Fluorine Chem. 128 (2007) 448.
[4] M. Al-Mamouri, P.P. Edwards, C. Greaves, M. Slaski, Nature (London) 369 (1994) 382.
[5] P.R. Slater, J.P. Hodges, M.G. Francesconi, C. Greaves, M. Slaski, J. Mater. Chem. 7 (1997) 2077.
[6] A.M. Abakumov, J. Hadermann, G. Van Tendeloo, R.V. Shpanchenko, P.N. Oleinikov, E.V. Antipov, J. Solid State Chem. 142 (1999) 440.
[7] C. Greaves, J.L. Kissick, M.G. Francesconi, L.D. Aiken, L.J. Gillie, J. Mater. Chem. 9 (1999) 111.
[8] G.S. Case, A.L. Hector, W. Leavson, R.L. Needs, M.F. Thomas, M.T. Weller, J. Mater. Chem. 9 (1999) 2821.
[9] F.J. Berry, X. Ren, R. Heap, P. Slater, M.F. Thomas, Solid State Commun. 134 (2005) 621.
[10] P.R. Slater, R.K.B. Gover, J. Mater. Chem. 11 (2001) 2035 and references therein.
[11] A.C. Larsen, R.B. Von Dreele, Los Alamos Laboratory Report, NO-LA-U-86-748, Los Alamos, NM, 2000.
[12] N. Binsted, EXCURV98, CCLRC Daresbury Labaratory Computer Program, 1998.
[13] J.D. Gale, Philos. Mag. B 73 (1997) 3;
J.D. Gale, J. Chem. Soc. Farad. Trans. 93 (1997) 629;
J.D. Gale, J. Phys. Chem. B 102 (1998) 5423.
[14] J.D. Gale, E.A. Moore, K.M. Yeowell, unpublished results.
[15] R.V. Shpanchenko, E.V. Antipov, L.M. Kovba, Zh. Neorg. Khim. 38 (1993) 599;
R. Heap, M.S. Islam, P.R. Slater, Dalton Trans. (2005) 460.
[16] M.A. Green, K. Prassides, P. Day, J.K. Stalick, Synth. Met. 71 (1995) 1617.
[17] M.A. Green, K. Prassides, P. Day, J.K. Stalick, J. Chem. Soc. Farad. Trans. 92 (1996) 2155.
[18] B.J. Kennedy, Aust. J. Chem. 50 (1997) 917.
[19] M. Le Floch-Durand, U. Haeberlen, C. Muller, Can. J. Phys. 43 (1982) 107.
[20] S. Chaudhuri, F. Wang, C.P. Grey, J. Am. Chem. Soc. 124 (2002) 11746.
[21] T.J. Kiczenski, J.F. Stebbins, J. Non-Cryst. Solids 306 (2002) 160.
[22] L.-S. Du, F. Wang, C.P. Grey, J. Solid State Chem. 140 (1998) 285.
[23] D. Dakternieks, H. Zhu, Organometallics 1120 (1992) 3820.
[24] M.J. Taylor, J.M. Coddington, Polyhedron 11 (1992) 1531.